


Wave Steering by Relaying Interface States in a Valley-Hall-Derived Photonic Superlattice

Hongchen Chu^{1,†}, Ze-Guo Chen^{2,*}, Yun Lai^{1,‡} and Guancong Ma^{2,3,§}

¹*National Laboratory of Solid State Microstructures, School of Physics and Collaborative Innovation Center of Advanced Microstructures, Nanjing University, Nanjing 210093, China*

²*Department of Physics, Hong Kong Baptist University, Kowloon Tong, Hong Kong, China*

³*Hong Kong Baptist University Institute of Research and Continuing Education, Shenzhen, China*

 (Received 5 June 2021; revised 5 August 2021; accepted 16 September 2021; published 6 October 2021)

Topological notions in physics have become a powerful perspective that leads to the discoveries of interface states. In this work, we present a scheme to steer waves by leveraging the properties of valley interface states (VISs) in a valley photonic crystal (VPC). Due to the chiral characteristics, the VISs deterministically possess either positive or negative dispersion relation, which can cause an obliquely incident wave to undergo a lateral shift. By stacking multiple VPC interfaces, the VIS-induced lateral shifts can relay in the transmitted wave towards the far side of incidence. By selectively engaging one type of VISs, the resultant outgoing wave appears to have undergone negative refraction. While this refraction can be flipped to positive by selectively exciting the other type of VISs with positive dispersion. This finding is verified in microwave experiments. Our scheme opens application scenarios for topological systems in wave manipulations.

DOI: [10.1103/PhysRevApplied.16.044006](https://doi.org/10.1103/PhysRevApplied.16.044006)

I. INTRODUCTION

Since its introduction to physics in the 1980s, the concept of topology has drastically changed our fundamental understanding of matters [1,2]. The profound insights brought about by topological notations have led to the discovery of a plethora of exotic phenomena. But perhaps none is more impactful than the deterministic prediction of interface states localized between two topologically distinct matters [3,4]. These topological interface states have the fascinating properties of being robust against disorder and sometimes immune to backscattering, making them an ideal candidate for transferring information or energy. In recent years, the exploration of topological notions in photonics and electromagnetism [5–7], and acoustics [8,9], have also unshackled our traditional understandings of these classical waves and led to exciting developments. The localized characteristics of topologically protected states make them a natural candidate for manipulating confined waves, e.g., at boundaries or interfaces. It is therefore not surprising that the potential of interface states for bulk-wave-steering applications has largely been ignored.

In parallel with the development of topological notions in classical wave systems, bulk-wave steering has witnessed great advancements in the past decades, thanks to the developments in wave-functional materials such as metamaterials. Among a kaleidoscopic collection of interesting and exotic wave phenomena, negative refraction was perhaps the fire that sparked the research boom and is still critically important in many intriguing applications like superlens. Negative refraction was obtained by negative effective index or suitable dispersion in metamaterials and wave crystals [10–25], phase gradient in metasurfaces [26–30], metasurfaces with parity-time symmetry [31–34], etc. However, so far topologically protected interface states have not been adopted to realize such bulk-wave steering like negative refraction. Here, we report a topological route to deterministically achieve negative or positive refraction of bulk waves by leveraging on the properties of valley interface states (VISs). Our approach is based on the VIS existing at zigzag interfaces of two-dimensional (2D) valley-Hall photonic crystal (VPC) [35–41]. The chirality of the VISs is uniquely associated with the cleavage at the interface. We show that with a specific cleavage at the interface, the VIS must possess a negative dispersion. As a result, an incident wave would experience a shift negative to the wave-vector component along the interface. By stacking such VPC interfaces to form a superlattice, multiple VISs can relay the incident wave towards the far side. Since the VISs exist in the bulk of

*zeguoc@foxmail.com

†These authors have contributed equally to this work.

‡laiyun@nju.edu.cn

§phgcma@hkbu.edu.hk

the superlattice, the resultant effect is the negative refraction of the incident wave. In microwave experiments, we observed pronounced negative refraction for the beam exiting at the far side of the VPC superlattice. Besides negative refraction, positive refraction can also be produced by using a different type of interface. Our work thus reveals that relaying VISs is a way to steer the bulk waves deterministically.

II. VISS WITH NEGATIVE AND POSITIVE DISPERSIONS IN VPC

We begin by considering a 2D VPC consisting of a honeycomb lattice of dielectric cylinders with relative permittivity $\epsilon_r = 12.97$ and radii $r = 0.3a/\sqrt{3}$ in air, where a is the lattice constant. We introduce inversion symmetry breaking by the parameter $\delta = (r_2 - r_1)/(r_1 + r_2)$, i.e., the difference in the radii of the two cylinders in one unit cell. This lifts the degeneracy of the Dirac cones and induces a local distribution of nonzero Berry curvature. As a result, integration of the Berry curvature near each valley gives rise to nonzero “valley Chern numbers” [42–44], which protect the existence of chiral VISs. We produce two types of supercells, denoted type A and B , which are mirror-symmetric counterparts of each other. We construct

a supercell strip that has N layers of type- B unit cells sandwiched by $N/2$ layers of type- A unit cells, as shown in Fig. 1(a). The supercell strip thus has two types of zigzag interfaces. The type-I interface, marked by the red dashed line [Fig. 1(a)], is joined by two smaller cylinders, whereas the type-II interface is joined by two larger cylinders [blue dashed line in Fig. 1(a)]. A bulk band gap is seen at the normalized frequency range of 0.26–0.32. Note that the valley Chern number is exactly quantized only when δ approaches zero, at which point the two chiral VISs form a linear crossing at the K (K') point [Figs. 1(b) and 1(c)]. Such a crossing indicates that the two VIS bands must have opposite dispersion, i.e., group velocity. However, the VISs persist even when δ is nonzero. This can be seen in Fig. 1(b), where we set $N = 8$. The increase of δ widens the bulk gap and smoothly deforms VIS bands. However, the tuning of δ leaves the bulk topological characteristics and existence of the two VISs intact. For the ease of experiments, which can benefit from a larger bulk gap, we set $\delta = 0.2$ by choosing the radii of the cylinders to $r_1 = 0.24a/\sqrt{3}$ and $r_2 = 0.36a/\sqrt{3}$ [red and blue dots in Fig. 1(a), respectively]. Importantly, the VIS at the type-I interface [red in Fig. 1(d)] has retained the negative dispersion for $|k_x| > 0.4$. This characteristic plays a crucial role in achieving negative refraction, which is explored later.

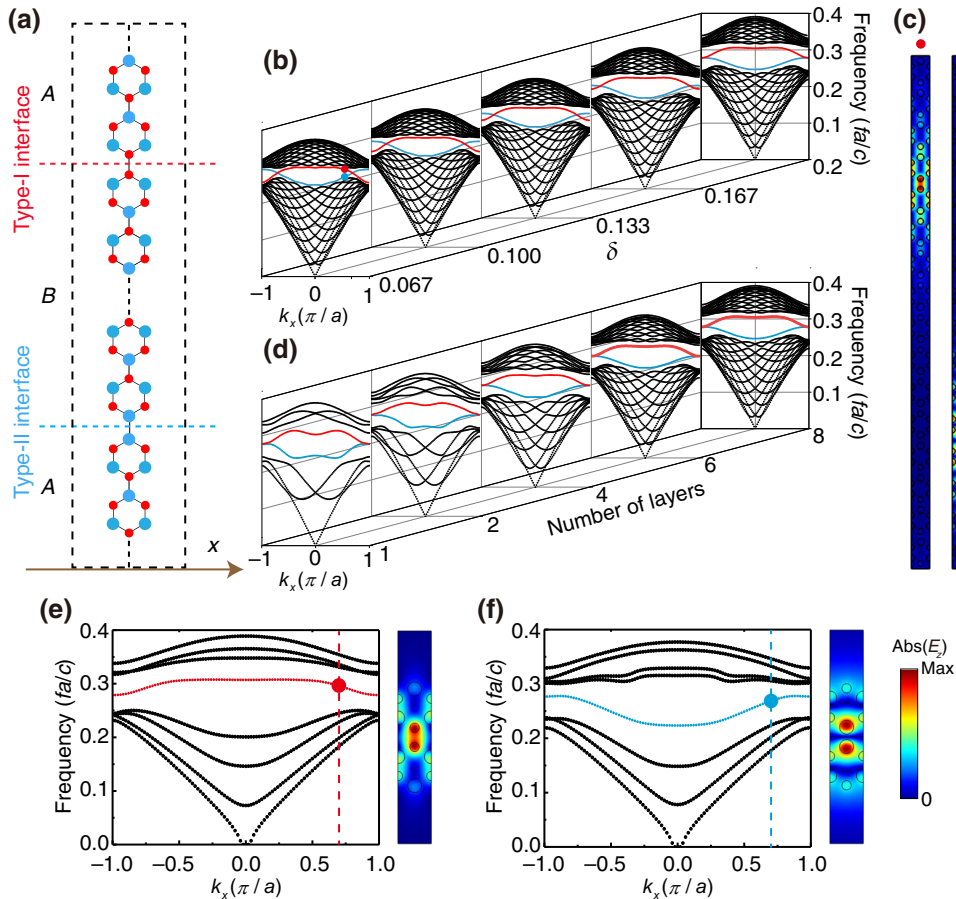


FIG. 1. (a) Schematic of a VPC strip containing two types of interface labeled by red and blue dashed lines. The topological protection of the VISs is shown in (b)–(f). (b) The projected band structure as a function of radius contrast shows VISs with different chirality, the red (blue) dots indicate the interface state where the corresponding field distribution is plotted in (c). (d) The projected band structure as a function of layer number. (e), (f) The interface state behaves well localized even when the system is only composed of two layers of VPCs with radiation boundary condition. The right inset shows the field distributions.

We further plot the band structure as a function of layer numbers in Fig. 1(d). Surprisingly, such VISs persist even when the strip contains only two unit cells (one of each type), as shown in Fig. 1(d). When the strip has only one type of interface, the corresponding VIS has deterministic dispersion, as shown in Figs. 1(e) and 1(f), where we introduce an experimentally feasible system with radiation boundary condition. Moreover, comparing Fig. 1(c) and the right panels in Figs. 1(e) and 1(f), it is seen that the in-gap modes retain their mode profiles, which is evidence that the VISs survive the reduction of unit cells. Such a characteristic has been leveraged to achieve a one-way interface transport of waves analogous to the valley-Hall effect [35]. The VIS field profiles show strongly localized distributions at the interface with an evanescent characteristic seen in the y direction. Such field profiles indicate a large real wave vector parallel to the interface and an imaginary wave vector in the normal direction.

We next examine the transmission of a wave incident on such a strip at the frequencies of the VISs. Consider a plane wave incident at an angle θ , as schematically shown in Figs. 2(a) and 2(d), we compute the transmission coefficients $t(f, \theta)$ for the frequencies inside the band gap and the incident angles $0^\circ < \theta < 60^\circ$. The results for both types of interfaces are, respectively, shown in Figs. 2(b) and 2(e). Large transmission is identified at specific frequencies and angles. By considering the conservation of momentum (wave vector) along the interface direction, we retrieve the dispersion relations from the transmission spectra [37], which aligns excellently with the VIS bands, as shown in Figs. 2(c) and 2(f). This evidence proves

that large transmission is possible by relaying the VISs, despite their individual evanescent characteristic. Indeed, the large transmission can be viewed as a generalization of extraordinary optical transmission [45–47], in which the contribution from surface plasmon polariton is replaced by the VISs.

III. RELAYING VISS FOR WAVE STEERING IN A VPC SUPERLATTICE

The chiral characteristic of the VISs at different interfaces enables an intriguing way to manipulate wave transmission. With a type-I interface [Fig. 2(a)], the VIS has negative dispersion in k_x . Such a VIS would transfer wave energy toward the negative direction of the wave vector along the interface. As a result, when an incident wave couples to this VIS, the wave gains a negative shift parallel to the interface and the beam exiting from the far side would appear to have undergone negative refraction. However, for the type-II interface, the incident wave would gain a positive shift parallel to the interface, appearing to undergo positive refraction. We numerically verify these findings by finite element (FEM) simulations. We employ a Gaussian beam incident at an angle of 45° , as shown in Fig. 3(a). At a normalized frequency of $fa/c = 0.307$, negative refraction behavior is observed for the type-I interface, as the center of the outgoing beam is shifted to the left side of the normal [right panel in Fig. 3(a)]. In contrast, positive refraction is seen for the type-II interface at a frequency of $fa/c = 0.233$, as shown in Fig. 3(b). The difference in frequency

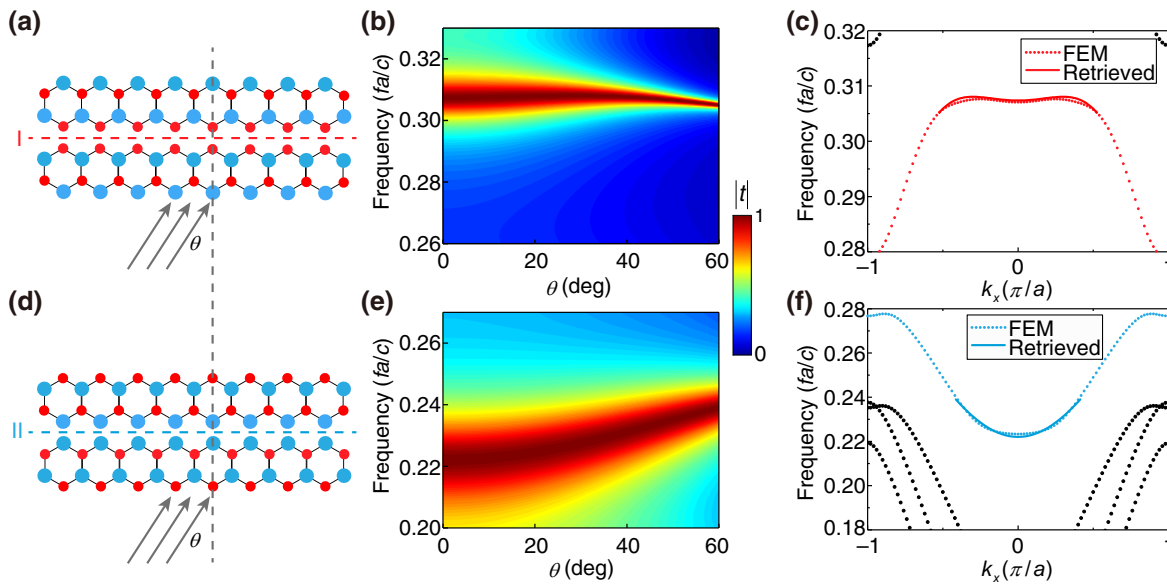


FIG. 2. Schematic drawing of a plane wave incident on a system with a type-I (a) and type-II (d) interface. Both systems have only two unit cells. (b), (e) The transmission spectra as functions of incidence angle θ and normalized frequency fa/c . The color represents the transmission amplitude. (c), (f) The VIS dispersions retrieved from the transmission spectra (red and blue solid curves) show excellent agreement with the band structures calculated by FEM (red and blue dots).

is due to the spectral mismatch of the VISs at different interfaces. We note that there is a certain amount of reflection for both cases, which is due to impedance mismatch and the fact that the incident Gaussian beam carries additional wave vectors deviating from the VISs at this frequency.

By stacking multiple type-I (type-II) VPC interfaces together, we obtain a superlattice as shown in Figs. 3(c) and 3(d). Although both type-I and type-II interfaces exist in the superlattice, the two types of VISs are mismatched in their frequency. By choosing the frequency of the incident wave, we can selectively excite only one type of VIS and suppress the other type. In this way, the oblique incident wave is relayed across the superlattice by only one type of VIS, resulting in a pronounced negative or positive shift in the outgoing beam, which depends on the dispersion of the chosen VISs. We take four layers of type-I (type-II) VPC interfaces as an example and calculate the field distribution by FEM simulations. Figures 3(c) and 3(d) show the calculated field distributions under the illumination of a Gaussian beam at an angle of 45° . The outgoing beam is significantly shifted to the left (right) side of the surface normal, giving rise to a pronounced negative (positive) refraction effect. The refraction behavior of electromagnetic waves in the relayed VPCs can also be understood from the aspect of coupled waveguides. We can treat the system as a coupled waveguide array consisting of neighboring one-layer-cladding waveguides. Both

full-wave simulations and later microwave experiments verify the efficient coupling of the edge modes, leading to the clear observation of bulk-wave refraction. We note that the desired positive or negative refraction is both derived by the topological properties of the edge states in infinite VPC systems. As shown in Fig. 3(e), we plot the bulk bands of this new superlattice. The two colored bands are the descendants of the VISs. Note that the dispersion characteristics of the two types of VISs are carried over to the bulk dispersion, with the red (blue) bands showing negative (positive) group velocity. Such a mechanism reveals a deterministic approach for finding edge modes with desired positive or negative dispersions to control bulk-wave refraction.

IV. EXPERIMENTAL VALIDATION

Finally, we demonstrate the VIS-induced positive and negative refraction by proof-of-principle microwave experiments. The VPCs consist of a honeycomb lattice of alumina ceramic ($\epsilon_r = 12.97$) cylinders with a height $h = 8$ mm and a is 9.21 mm. The simulated electric field distributions E_z for VPC superlattices with four layers of type-I and type-II interfaces are, respectively, shown in Figs. 4(a) and 4(d), where negative refraction and positive refraction are both clearly observed. In the experiments, the VPCs are assembled inside a parallel-plate waveguide composed of two flat aluminum plates, as shown in Fig. 4(b), where the

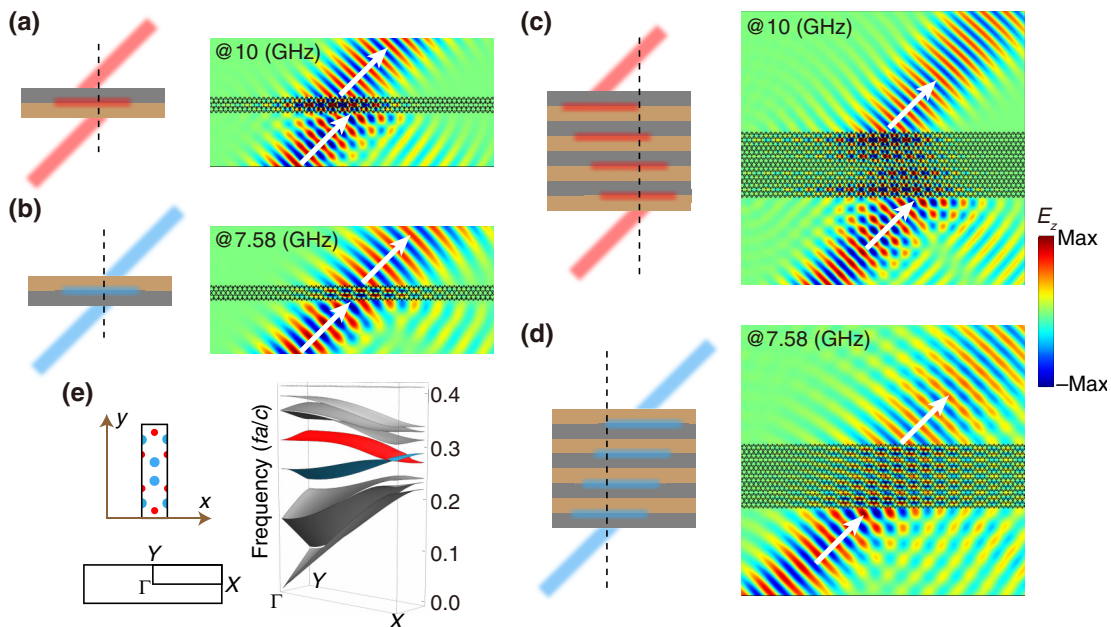


FIG. 3. Schematic and simulation result of a two-layer system supporting transmission extreme where the transmitted wave performs as negative (a) or positive (b) refracted, depending on the type of the excited VIS. The length of the system along the interface direction is $60a$. The white arrows indicate the direction of energy flow. (c), (d) Schematic and simulation result of a multiple-layer system supporting negative (c) and positive (d) refraction. (e) The stacking procedure produces a new PC with a larger unit cell, where its band structure is plotted. The red and blue band results from the interface state shown in (a) and (b), respectively.

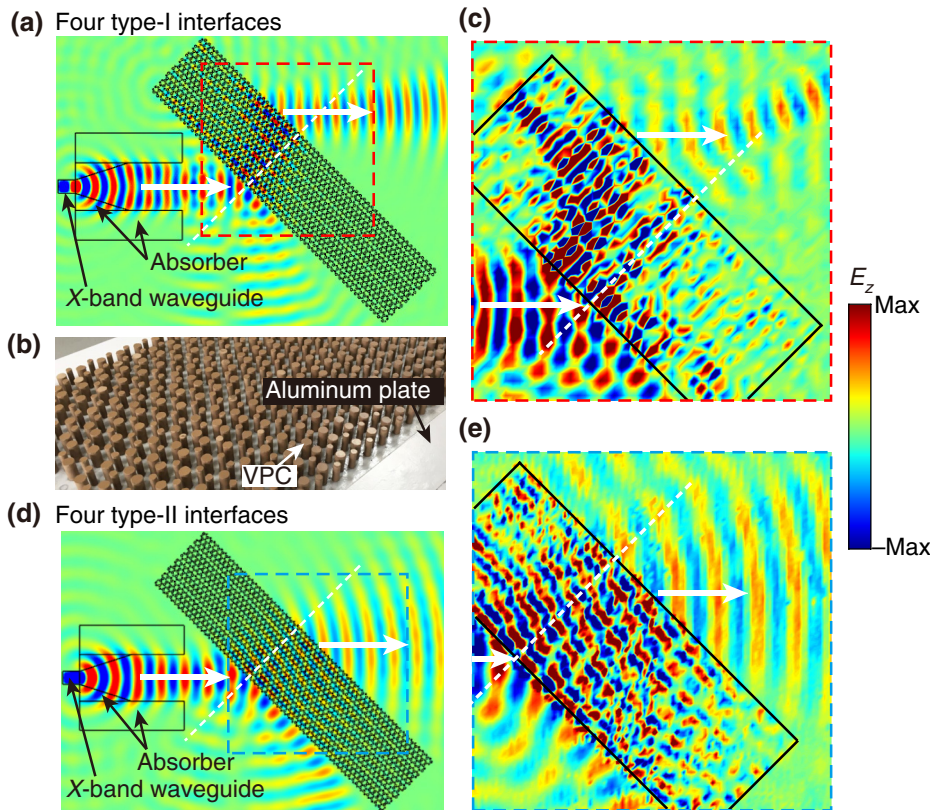


FIG. 4. Experimental demonstration of negative and positive refraction by relaying VISs. (a), (d) Simulated field distributions of VPCs with four type-I (a) and type-II (d) interfaces. Dashed boxes depict the measured region in experiments. The incident beam is generated by a standard X -band waveguide along with absorber materials. (b) The photo of the fabricated VPC superlattice consisting of alumina ceramic cylinders. (c), (e) Measured field distributions of negative refraction through VPC with four type-I interfaces (c) and positive refraction through VPC with four type-II interfaces (e).

upper plate is not shown. A standard X -band waveguide and microwave-absorbing materials are used to generate a beam with finite width. The lower metal plate, the VPCs, and the beam generator are mounted on a 2D motorized translational stage. A tiny gap of 0.7 mm is introduced between the upper plate and the top of the VPCs so that the upper plate does not impede the scanning. The electric fields are measured via an antenna fixed in a hole in the upper plate. The emitting X -band waveguide and the probing antenna are connected to a KEYSIGHT N5224B network analyzer to acquire the transmitted magnitude and phase of microwave signals. The measured electric field distributions of VPC with four-layer type-I interfaces at frequency 11.32 GHz are shown in Fig. 4(c). It is clearly seen that the transmitted wave is shifted to the left side of the surface normal, which is consistent with the simulation results obtained by FEM in Fig. 4(a). Specifically, in Fig. 4(c), we see the measured fields inside the VPC have a layered pattern, which implies the excitation and relay of the VISs. These results prove our prediction of negative refraction by relaying VISs. On the other hand, Fig. 4(e) shows the measured electric field distributions at frequency 8.80 GHz, in which positive refraction is observed to be in excellent agreement with the simulation results shown in Fig. 4(d). The discrepancy between the numerical and experimental results shown in Fig. 4 is attributed to the following reasons. The first one is the inevitable fabrication error in the alumina ceramic cylinders of VPCs. The

second one is the deviations in the placement of the cylinders, which are arranged by hand. The third reason is the air gap between the VPCs and the upper waveguide plate, which is introduced for the convenience of field scanning. In addition, due to the space limitation in our apparatus, the total size of the VPCs in experiments is smaller than that in simulations, which can generate reflections of VISs by the lateral boundaries of the VPC system. Despite these experimental disturbances, the positive and negative refraction in the numerical and experimental results are clearly consistent with each other and the theoretical prediction.

V. CONCLUSION

In conclusion, we propose and demonstrate an unusual strategy by stacking VPC interfaces, each sustaining a VIS to realize the negative refraction between the VPC superlattice and the background medium. Strikingly, although our mechanism is underpinned by VISs with negative dispersion, the corollary outcome is a wave-steering effect in bulks of the superlattice. Therefore, our results hint that the functionality of VISs can go beyond interface-wave manipulation. Meanwhile, it is worth noting that the VPC superlattice can also be analyzed by using the equifrequency contour of its bulk bands, which also indicates negative dispersion. Such negative bulk bands are revealed to have a topological origin, which dictates that

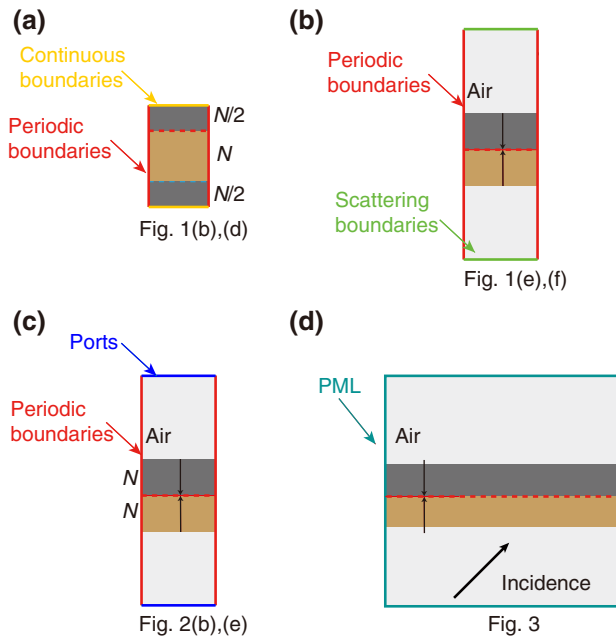


FIG. 5. Setups for the different simulations in the main text. The corresponding figure labels are shown at the bottom of the corresponding setup.

the VPC interface must support two types of VISs with opposite chirality, and VISs with negative dispersions are guaranteed to exist. Consequently, our scheme does not rely on specific parameters and is deterministic. Our design

is thus fundamentally different from existing routes to negative refraction in metamaterials and metasurfaces requiring delicate design of effective indices or phase gradients. Our work also differs from the previous Fermi-arc-induced negative refraction, which guides waves along different surfaces of a three-dimensional Weyl system [48,49]. Lastly, the relaying mechanism is not restricted to valley-Hall systems. It can also be achieved in other types of topological phases such as the Chern insulator model [50,51], the 2D Su-Schrieffer-Heeger model [52,53], quantum spin Hall systems [54], and so on, where time-reversal symmetry, chiral symmetry or mirror symmetry will ensure the appearance of interface states with deterministic dispersion, depending on the model, see one example in Appendix C. The mechanism can also be adapted for a wide variety of wave systems such as acoustic waves, elastic waves, and optics.

ACKNOWLEDGMENTS

Z.-G.C. thanks Xiao Hu, Cheng He and Xiao-Chen Sun for helpful discussions. This work is supported by Hong Kong Research Grants Council (Grants No. 12302420, No. 12300419, No. 22302718, No. C6013-18G), National Natural Science Foundation of China (Grants No. 11922416, No. 11802256), and Hong Kong Baptist University (Grants No. RC-SGT2/18-19/SCI/006). Y. L. also acknowledges financial support from the National Key R&D Program of

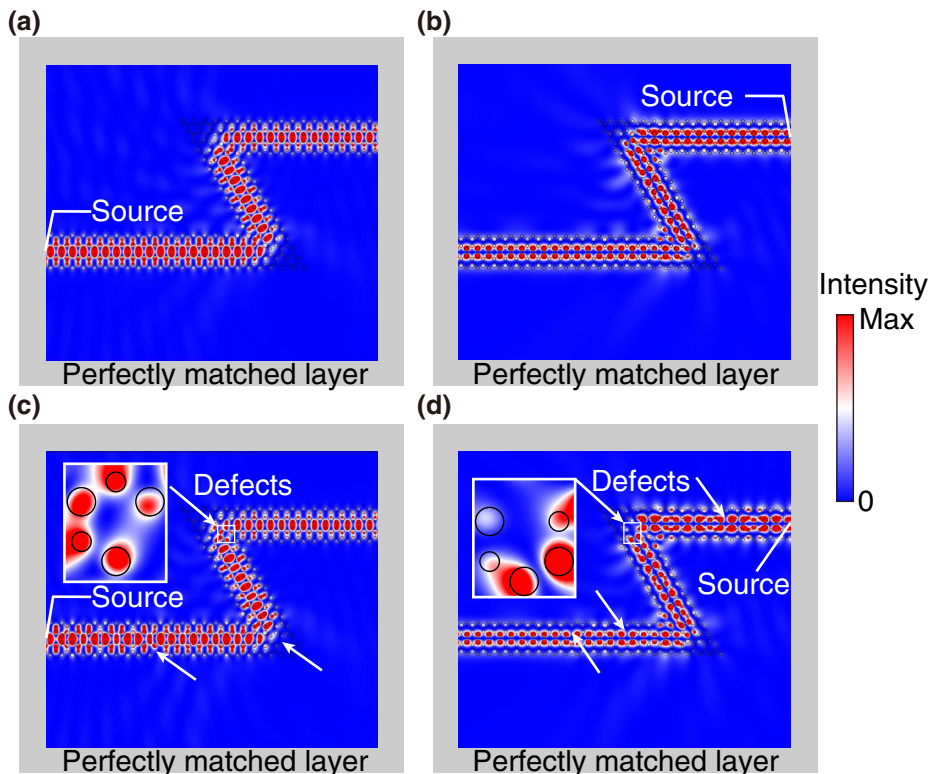


FIG. 6. (a) Propagation of the VIS on the type-I interface. (b) Propagation of the VIS on the type-II interface. (c) Propagation of the VIS on the type-I interface with three dielectric cylinders of the VPCs removed. (d) Propagation of the VIS on the type-II interface with four dielectric cylinders of the VPCs removed.

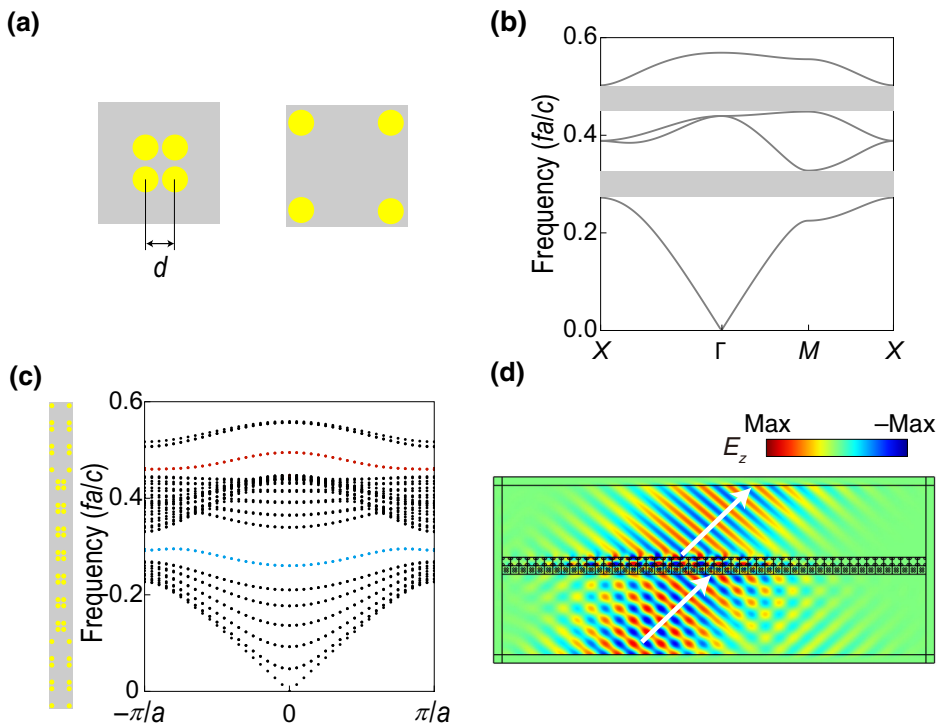


FIG. 7. Interface states that appear in square lattices can also realize negative refraction. (a) The system is a square lattice of dielectric cylinders with relative permittivity $\epsilon_r = 12.97$. The two structures produce the same band structure shown in (b) with two bulk band gaps. The radius of the cylinder is $0.12a$, the nearest distance of the cylinders is $2a/7$. (c) Two kinds of interface states exist in the two bulk band gaps. (d) The interface state with negative dispersion can induce negative refraction.

China (Grant No. 2020YFA0211300), the National Natural Science Foundation of China (Grant No. 11974176, 61671314).

APPENDIX A: SIMULATION DETAILS

Different simulation setups are used in the main text to explain the interface state evolution under different boundary conditions. Figure 5 summarizes all the setups.

APPENDIX B: THE PROPAGATION OF THE VISS

To verify the topology origin of the VISSs, we simulate the wave propagation along the interface of VPCs, as shown in Figs. 6(a) and 6(b). It is seen that the wave can propagate through sharp bending corners without much scattering. In Figs. 6(c) and 6(d), scattering defects are included by removing several dielectric cylinders of the VPCs. The interfacial propagation is unaffected by the presence of the defects, which is similar to a standard valley Hall system, where only scattering from K state to K' state is supported, which can be avoided by source symmetry or system symmetry engineering.

APPENDIX C: A 2D SQUARE LATTICE CASE

Here, we show a different example to demonstrate the deterministic characteristics of our design route. As shown in Fig. 7, we study 2D square lattice PCs that support interface states protected by nonzero bulk dipole polarization. The topological physics is captured by the 2D Su-Schrieffer-Heeger (SSH) model [52,53]. In 2D SSH

model, the system supports two kinds of interface states in two bulk band gaps. Due to the chiral symmetry, the two in-gap states exhibit different dispersions, i.e., one is positive and the other one is negative (this is another example to show our scheme based on topology physics is deterministic). The in-gap states exhibiting negative dispersion can also be utilized to realize negative refraction as shown in Fig. 7(d). This example, together with the VPC case, shows that a pair of interface states with opposite dispersions can deterministically appear in more than one type of topological lattice. More examples can be found. For instance, Chern insulators exhibiting chiral interface states, whose chirality is related to the direction of the magnetic field; the topological photonic crystalline insulators exhibiting pairs of interface states protected by time-reversal symmetry or chiral symmetry, etc. As such, topological physics is providing a different perspective and a systematic route to obtain interface states with opposite dispersions. Such an approach guides us to realize wave-steering functionalities on demand.

- [1] D. J. Thouless, M. Kohmoto, M. P. Nightingale, and M. den Nijs, Quantized Hall Conductance in a Two-Dimensional Periodic Potential, *Phys. Rev. Lett.* **49**, 405 (1982).
- [2] F. D. Haldane, Model for a Quantum Hall Effect Without Landau Levels: Condensed-Matter Realization of the “Parity Anomaly”, *Phys. Rev. Lett.* **61**, 2015 (1988).
- [3] X. L. Qi and S. C. Zhang, Topological insulators and superconductors, *Rev. Mod. Phys.* **83**, 1057 (2011).
- [4] M. Z. Hasan and C. L. Kane, Topological insulators, *Rev. Mod. Phys.* **82**, 3045 (2010).

- [5] L. Lu, J. D. Joannopoulos, and M. Soljačić, Topological photonics, *Nat. Photonics* **8**, 821 (2014).
- [6] A. B. Khanikaev and G. Shvets, Two-dimensional topological photonics, *Nat. Photonics* **11**, 763 (2017).
- [7] T. Ozawa, H. M. Price, A. Amo, N. Goldman, M. Hafezi, L. Lu, M. C. Rechtsman, D. Schuster, J. Simon, and O. Zilberberg, Topological photonics, *Rev. Mod. Phys.* **91**, 15006 (2019).
- [8] X. Zhang, M. Xiao, Y. Cheng, M. Lu, and J. Christensen, Topological sound, *Commun. Phys.* **1**, 1 (2018).
- [9] G. Ma, M. Xiao, and C. T. Chan, Topological phases in acoustic and mechanical systems, *Nat. Rev. Phys.* **1**, 281 (2019).
- [10] V. G. Veselago, The electrodynamics of substances with simultaneously negative values of ϵ and μ , *Sov. Phys. Usp.* **10**, 509 (1968).
- [11] J. B. Pendry, Negative Refraction Makes a Perfect Lens, *Phys. Rev. Lett.* **85**, 3966 (2000).
- [12] D. R. Smith, W. J. Padilla, D. C. Vier, S. C. Nemat-Nasser, and S. Schultz, Composite Medium with Simultaneously Negative Permeability and Permittivity, *Phys. Rev. Lett.* **84**, 4184 (2000).
- [13] R. A. Shelby, D. R. Smith, and S. Schultz, Experimental verification of a negative index of refraction, *Science* **292**, 77 (2001).
- [14] D. R. Smith and N. Kroll, Negative Refractive Index in Left-Handed Materials, *Phys. Rev. Lett.* **85**, 2933 (2000).
- [15] V. M. Shalaev, Optical negative-index metamaterials, *Nat. Photonics* **1**, 41 (2007).
- [16] D. R. Smith and D. Schurig, Electromagnetic Wave Propagation in Media with Indefinite Permittivity and Permeability Tensors, *Phys. Rev. Lett.* **90**, 77405 (2003).
- [17] D. R. Smith, D. Schurig, J. J. Mock, P. Kolinko, and P. Rye, Partial focusing of radiation by a slab of indefinite media, *Appl. Phys. Lett.* **84**, 2244 (2004).
- [18] A. J. Hoffman, L. Alekseyev, S. S. Howard, K. J. Franz, D. Wasserman, V. A. Podolskiy, E. E. Narimanov, D. L. Sivco, and C. Gmachl, Negative refraction in semiconductor metamaterials, *Nat. Mater.* **6**, 946 (2007).
- [19] J. Yao, Z. Liu, Y. Liu, Y. Wang, C. Sun, G. Bartal, A. M. Stacy, and X. Zhang, Optical negative refraction in bulk metamaterials of nanowires, *Science* **321**, 930 (2008).
- [20] S. Guan, S. Y. Huang, Y. Yao, and S. A. Yang, Tunable hyperbolic dispersion and negative refraction in natural electric materials, *Phys. Rev. B* **95**, 165436 (2017).
- [21] C. Luo, S. G. Johnson, J. D. Joannopoulos, and J. B. Pendry, All-angle negative refraction without negative effective index, *Phys. Rev. B* **65**, 201104 (2002).
- [22] E. Cubukcu, K. Aydin, E. Ozbay, S. Foteinopoulou, and C. M. Soukoulis, Negative refraction by photonic crystals, *Nature* **423**, 604 (2003).
- [23] P. V. Parimi, W. T. Lu, P. Vodo, and S. Sridhar, Photonic crystals: Imaging by flat lens using negative refraction, *Nature* **426**, 404 (2003).
- [24] A. Berrier, M. Mulot, M. Swillo, M. Qiu, L. Thylen, A. Talneau, and S. Anand, Negative Refraction at Infrared Wavelengths in a two-Dimensional Photonic Crystal, *Phys. Rev. Lett.* **93**, 73902 (2004).
- [25] P. V. Parimi, W. T. Lu, P. Vodo, J. Sokoloff, J. S. Derov, and S. Sridhar, Negative Refraction and Left-Handed Electromagnetism in Microwave Photonic Crystals, *Phys. Rev. Lett.* **92**, 127401 (2004).
- [26] N. Yu, P. Genevet, M. A. Kats, F. Aieta, J. P. Tetienne, F. Capasso, and Z. Gaburro, Light propagation with phase discontinuities: Generalized laws of reflection and refraction, *Science* **334**, 333 (2011).
- [27] X. Ni, N. K. Emani, A. V. Kildishev, A. Boltasseva, and V. M. Shalaev, Broadband light bending with plasmonic nanoantennas, *Science* **335**, 427 (2012).
- [28] A. V. Kildishev, A. B. Oltasseva, and V. M. Shalaev, Planar photonics with metasurfaces, *Science* **339**, 1232009 (2013).
- [29] N. Yu and F. Capasso, Flat optics with designer metasurfaces, *Nat. Mater.* **13**, 139 (2014).
- [30] Y. Xu, Y. Fu, and H. Chen, Planar gradient metamaterials, *Nat. Rev. Mat.* **1**, 16067 (2016).
- [31] R. Fleury, D. L. Sounas, and A. Alù, Negative Refraction and Planar Focusing Based on Parity-Time Symmetric Metasurfaces, *Phys. Rev. Lett.* **113**, 23903 (2014).
- [32] F. Monticone, C. A. Valagiannopoulos, and A. Alù, Parity-Time Symmetric Nonlocal Metasurfaces: All-Angle Negative Refraction and Volumetric Imaging, *Phys. Rev. X* **6**, 41018 (2016).
- [33] J. Luo, J. Li, and Y. Lai, Electromagnetic Impurity-Immunity Induced by Parity-Time Symmetry, *Phys. Rev. X* **8**, 1 (2018).
- [34] J. Lan, X. Zhang, L. Wang, Y. Lai, and X. Liu, Bidirectional acoustic negative refraction based on a pair of metasurfaces with both local and global PT-symmetries, *Sci. Rep.* **10**, 10794 (2020).
- [35] T. Ma and G. Shvets, All-Si valley-Hall photonic topological insulator, *New J. Phys.* **18**, 25012 (2016).
- [36] J. Dong, X. Chen, H. Zhu, Y. Wang, and X. Zhang, Valley photonic crystals for control of spin and topology, *Nat. Mater.* **16**, 298 (2017).
- [37] X. Wu, Y. Meng, J. Tian, Y. Huang, H. Xiang, D. Han, and W. Wen, Direct observation of valley-polarized topological edge states in designer surface plasmon crystals, *Nat. Commun.* **8**, 1 (2017).
- [38] Y. Kang, X. Ni, X. Cheng, A. B. Khanikaev, and A. Z. Genack, Pseudo-spin–valley coupled edge states in a photonic topological insulator, *Nat. Commun.* **9**, 1 (2018).
- [39] F. Gao, H. Xue, Z. Yang, K. Lai, Y. Yu, X. Lin, Y. Chong, G. Shvets, and B. Zhang, Topologically protected refraction of robust kink states in valley photonic crystals, *Nat. Phys.* **14**, 140 (2018).
- [40] J. Noh, S. Huang, K. P. Chen, and M. C. Rechtsman, Observation of Photonic Topological Valley Hall Edge States, *Phys. Rev. Lett.* **120**, 63902 (2018).
- [41] M. I. Shalaev, W. Walasik, A. Tsukernik, Y. Xu, and N. M. Litchinitser, Robust topologically protected transport in photonic crystals at telecommunication wavelengths, *Nat. Nanotechnol.* **14**, 31 (2019).
- [42] A. Rycerz, J. Tworzydło, and C. W. J. Beenakker, Valley filter and valley valve in graphene, *Nat. Phys.* **3**, 172 (2007).

- [43] D. Xiao, W. Yao, and Q. Niu, Valley-contrasting Physics in Graphene: Magnetic Moment and Topological Transport, *Phys. Rev. Lett.* **99**, 236809 (2007).
- [44] K. Qian, D. J. Apigo, C. Prodan, Y. Barlas, and E. Prodan, Topology of the valley-Chern effect, *Phys. Rev. B* **98**, 155138 (2018).
- [45] T. W. Ebbesen, H. J. Lezec, H. F. Ghaemi, T. Thio, and P. A. Wolff, Extraordinary optical transmission through sub-wavelength hole arrays, *Nature* **391**, 667 (1998).
- [46] L. Martin-Moreno, F. J. Garcia-Vidal, H. J. Lezec, K. M. Pellerin, T. Thio, J. B. Pendry, and T. W. Ebbesen, Theory of Extraordinary Optical Transmission Through Subwavelength Hole Arrays, *Phys. Rev. Lett.* **86**, 1114 (2001).
- [47] H. Liu and P. Lalanne, Microscopic theory of the extraordinary optical transmission, *Nature* **452**, 728 (2008).
- [48] H. He, C. Qiu, L. Ye, X. Cai, X. Fan, M. Ke, F. Zhang, and Z. Liu, Topological negative refraction of surface acoustic waves in a Weyl phononic crystal, *Nature* **560**, 61 (2018).
- [49] T. Chen, J. Jiao, H. Dai, and D. Yu, Acoustic weyl points in a square lattice, *Phys. Rev. B* **98**, 214110 (2018).
- [50] Z. Wang, Y. D. Chong, J. D. Joannopoulos, and M. Soljacic, Reflection-Free One-Way Edge Modes in a Gyromagnetic Photonic Crystal, *Phys. Rev. Lett.* **100**, 13905 (2008).
- [51] H. Lai, H. Chen, B. He, C. He, and Y. Chen, Symmetrical and anti-symmetrical topological edge states based on two-dimensional magneto-optical photonic crystals, *Aip Adv.* **10**, 65029 (2020).
- [52] Z. Chen, C. Xu, R. Al Jahdali, J. Mei, and Y. Wu, Corner states in a second-order acoustic topological insulator as bound states in the continuum, *Phys. Rev. B* **100**, 75120 (2019).
- [53] B. Y. Xie, G. X. Su, H. F. Wang, H. Su, X. P. Shen, P. Zhan, M. H. Lu, Z. L. Wang, and Y. F. Chen, Visualization of Higher-Order Topological Insulating Phases in Two-Dimensional Dielectric Photonic Crystals, *Phys. Rev. Lett.* **122**, 233903 (2019).
- [54] L. H. Wu and X. Hu, Scheme for Achieving a Topological Photonic Crystal by Using Dielectric Material, *Phys. Rev. Lett.* **114**, 223901 (2015).